Research Article Vol. 58, No. 29 / 10 October 2019 / Applied Optics 7957

applied optics

Optimal position of an emitter in a wavelength-scale parabolic reflector

Harry Penketh,* Jacopo Bertolotti, and William L. Barnes

Department of Physics and Astronomy, University of Exeter, Exeter, Devon EX4 4QL, UK
**Corresponding author: hp289@exeter.ac.uk*

Received 27 May 2019; revised 26 July 2019; accepted 28 August 2019; posted 29 August 2019 (Doc. ID 368668); published 4 October 2019

We investigate the optimum emitter position within reflecting parabolic antennas whose size is comparable to the emission wavelength. Using finite-element modeling we calculate the dependence of the amount of power directed into a 20° half-angle cone on the emitter's position and compare with results obtained using geometrical optics. The spatially varying density of states within the wavelength-scale reflector is mapped and its impact discussed. In addition, it is demonstrated that changing the characteristic size of the reflector within the range from 0.5 to 1.5 times the emission wavelength has a strong bearing on the optimum emitter position, a position that does not in general coincide with the parabola's focus. We calculate that the optimal antenna size and emitter position allow for the maximum directed power to exceed that obtained in the geometrical optics regime.

https://doi.org/10.1364/AO.58.007957

1. INTRODUCTION

The parabolic reflector is one of the most popular and important means of generating highly directional radiation. At the macroscale, the broadband characteristics and simple design of parabolic reflectors have made them part of our daily lives, from automotive headlights and satellite dishes [1,2] to confocal microscopy and optical single-molecule spectroscopy [3,4]. Recently, the desire for highly directional radiation has seen this familiar concept applied to nanoscale sources of light, where the size of the reflector is comparable to the wavelength of emission [5–8]. As the reflector size decreases, the effects of interference, diffraction, and changes in the optical density of states (DOS) produce a deviation in the total radiated power and its directionality from the solution provided by the geometrical optics approximation [2,9–11].

The ability to locate and subsequently fabricate the reflector around a single-photon source has enabled precise alignment of the emitter with the geometrical focus of the reflector [5,6]. Here we explore, through finite-element modeling, the effect of emitter position within the parabola on the directionality and emitted power as the parabola size is reduced down to subwavelength sizes.

A paraboloid of revolution has the remarkable property that all incident rays parallel to the central axis will be reflected to the focus, making it the ideal shape to collect a collimated beam or to generate one starting from a point source. Figure 1 shows a simplified scheme of such a parabolic antenna.

The geometrical optics picture breaks down when the typical size of the parabolic antenna (or the distance between the emitter and the reflective surface) is comparable with the wavelength. At these scales, interference between the emitter and reflected waves plays a major role, modifying both its angular distribution and the total power radiated [12]. This latter effect, an entirely classical phenomenon, is usually associated with the local density of optical states [13]. Mapping the impact of the emitter position and reflector size on the radiated power is an integral part of understanding the emission of light using wavelength-scale parabolic reflectors and is the subject of this paper.

2. METHOD

To determine the impact of the emitter position within the reflector on the resulting radiation, we calculated the far-field pattern as a function of the position and orientation of a dipole emitter. Finite-element modeling software COMSOL Multiphysics (5.3a) was used to obtain far-field radiation patterns for emission from nanoscale and, for comparison, macroscale (geometrical optics regime) parabolic antennas [14]. We have chosen the power directed into a 20° half-angle right circular cone in the far field as a useful measure of the "performance" of the reflector. The cone and paraboloid share a common central axis and vertex. The resulting patterns were then post-processed using MATLAB R2018a to determine the power coupled into the cone.

An example of a far-field radiation pattern is shown in Fig. 2(b), with its corresponding local field distribution in Fig. 2(a). In Fig. 2(b) the dashed white circle marks the 20° half-angle cone within which the radiated power is integrated to quantify the performance of the reflector.

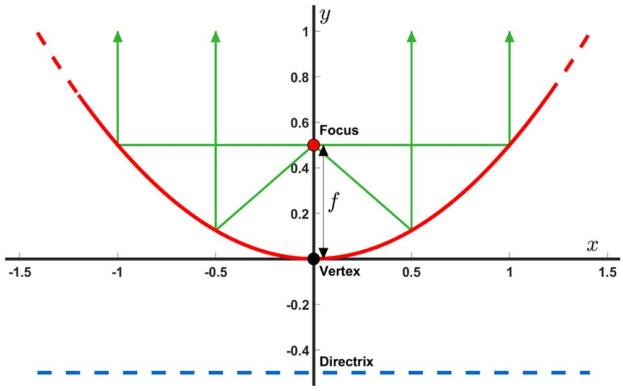

Fig. 1. A section of an infinite parabola (red) on Cartesian axes, defined by being equidistant from both the focus (red dot) and the directrix (blue, dashed) at all points. The distance from vertex to the focal point is the focal length f. Emission from the focal point (green lines) is collimated by specular refection from a parabolic surface.

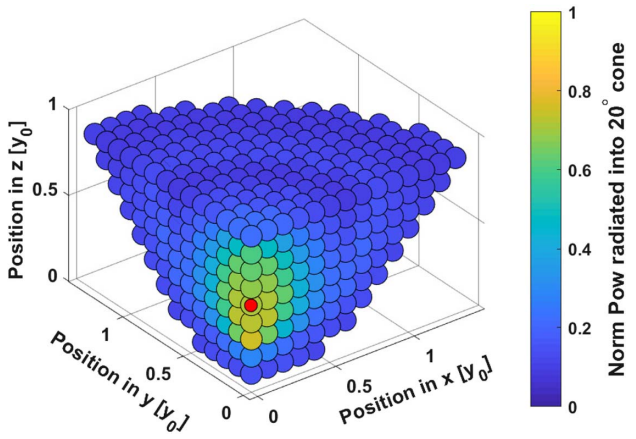

Fig. 3. Geometrical optics solution for power directed into a 20° half-angle cone for an isotropic emitter at varying positions within a finite parabolic reflector. As the solution is independent of the size of the reflector in the geometrical optics regime, the dimensions are given in terms of the vertex to opening distance y_0. Power values are normalized to the total emitted power. The red dot marks the focus of the paraboloid.

For the case of the macroscale paraboloids (size ≫ wavelength), radiation patterns were obtained using COMSOL's Geometrical Optics Module (Ray Tracing study). In a three-dimensional simulation, isotropic emission was released from a point within a finite-height reflecting paraboloid defined by the equation $z = (x^2 + y^2)/2$, with $x \in (-\sqrt{2}, \sqrt{2})$, $y \in (-\sqrt{2}, \sqrt{2})$, and $z \in (0, 1)$, with a perfect reflection boundary condition. The simulation domain was closed with a hemispherical boundary over the open portion of the paraboloid. The "freeze" boundary condition was applied here to terminate rays propagating into the far field. Wave vectors from rays frozen on this boundary were then used to obtain a far-field radiation pattern. Exploiting the radial symmetry present, this process was repeated for a regular two-dimensional grid of source positions, sampling the area within the parabola on one side of its central axis of symmetry. A "normal" physics-controlled mesh was used throughout.

For the wavelength-scale paraboloids, a frequency-domain study within COMSOL's Electromagnetic Waves, Frequency Domain module (Frequency Domain study) was used. The position and orientation of an oscillating electric point dipole was swept within a reflective paraboloid of revolution with the same shape as in the macroscale case. For a dipole moment perpendicular to the central axis of the reflector, a three-dimensional sweep of one quadrant of the reflector is required, while for the case of a dipole moment oscillating parallel to this axis, a two-dimensional sweep over $r = \sqrt{x^2 + y^2}$ and z is sufficient.

The paraboloid was designed to have a height of λ_0 and a radius at its opening of $\sqrt{2}\lambda_0$, with a design wavelength $\lambda_0 = 600$ nm. To produce the results of Fig. 5(a), the emission wavelength λ was varied between $0.5\lambda_0$ and $1.5\lambda_0$. As COMSOL employs the Stratton–Chu method [15–18] to transform from the near field to the far field, it is necessary

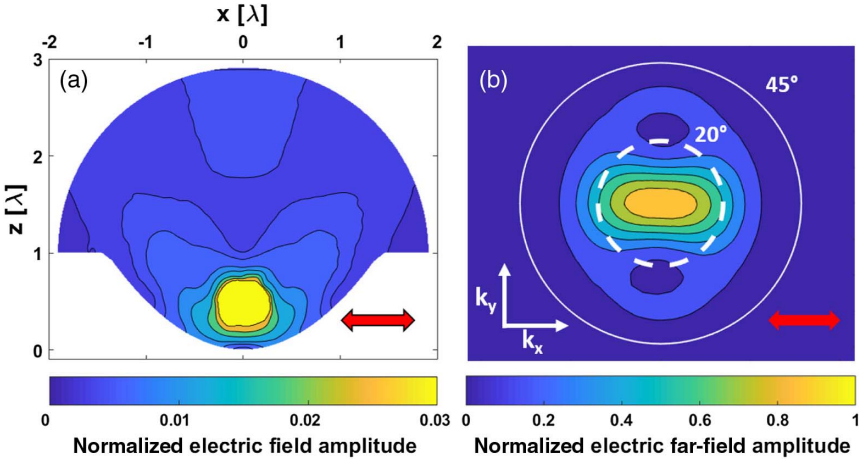

Fig. 2. (a) Contour plot of the calculated electric field amplitude in the $y = 0$ plane, surrounding an oscillating electric point dipole within a nanoscale parabolic reflector. The emission wavelength $\lambda = 600$ nm. The dipole is located at the parabola's focus (on axis at $z = 0.5\lambda$) and is oscillating in the $\hat{x}$ direction as indicated by the red arrow. The amplitude of the field has been normalized to unity. (b) Corresponding far-field contour plot, in wave-vector (k_x, k_y) space. The amplitude of the far field has been normalized to unity. The white circles mark emission inclination angles as labeled, with the dashed circle corresponding to the 20° half-angle cone used to measure the performance of the reflector.

to enclose the whole system in a closed surface with uniform properties. The reflecting parabolic surface was continued by a horizontal annulus of width $0.2\lambda_0$, which formed a closed surface with a hemisphere below the paraboloid. The perfect electric conductor boundary condition was applied to this entire surface. This allows an additional spherical air layer of annular radius $0.3\lambda_0$ to act both as the homogeneous boundary for the near-tofar-field transformation and a second-order scattering boundary condition (which effectively releases radiation from the simulation domain) on its outer surface. A "normal" physics-controlled mesh was used throughout.

3. RESULTS AND DISCUSSION

As a baseline to assess the emission characteristics of sources within wavelength-scale parabolic reflectors, we first calculated the geometrical optics solution. Figure 3 shows the variation in the power directed into a 20° half-angle cone as the source position is varied, simulated using the geometrical optics approximation. As expected, a region of efficient coupling into the target cone is found when the source is near the focus of the reflector. This efficiency remains below 100%, as the reflector is of finite extent. It is also noteworthy that the focus is not the optimum position for a source, even within the geometrical optics approximation; this is a consequence of both the finite extent of the paraboloid and the finite collection angle. While a source at the focus still optimizes emission on axis, emission into the cone is optimized when the source lies below the focal point as seen in Fig. 3.

With the macroscale solution established, we may now examine the wavelength-scale scenario. At this scale, the dipolar nature of an individual emitter must be taken into account.

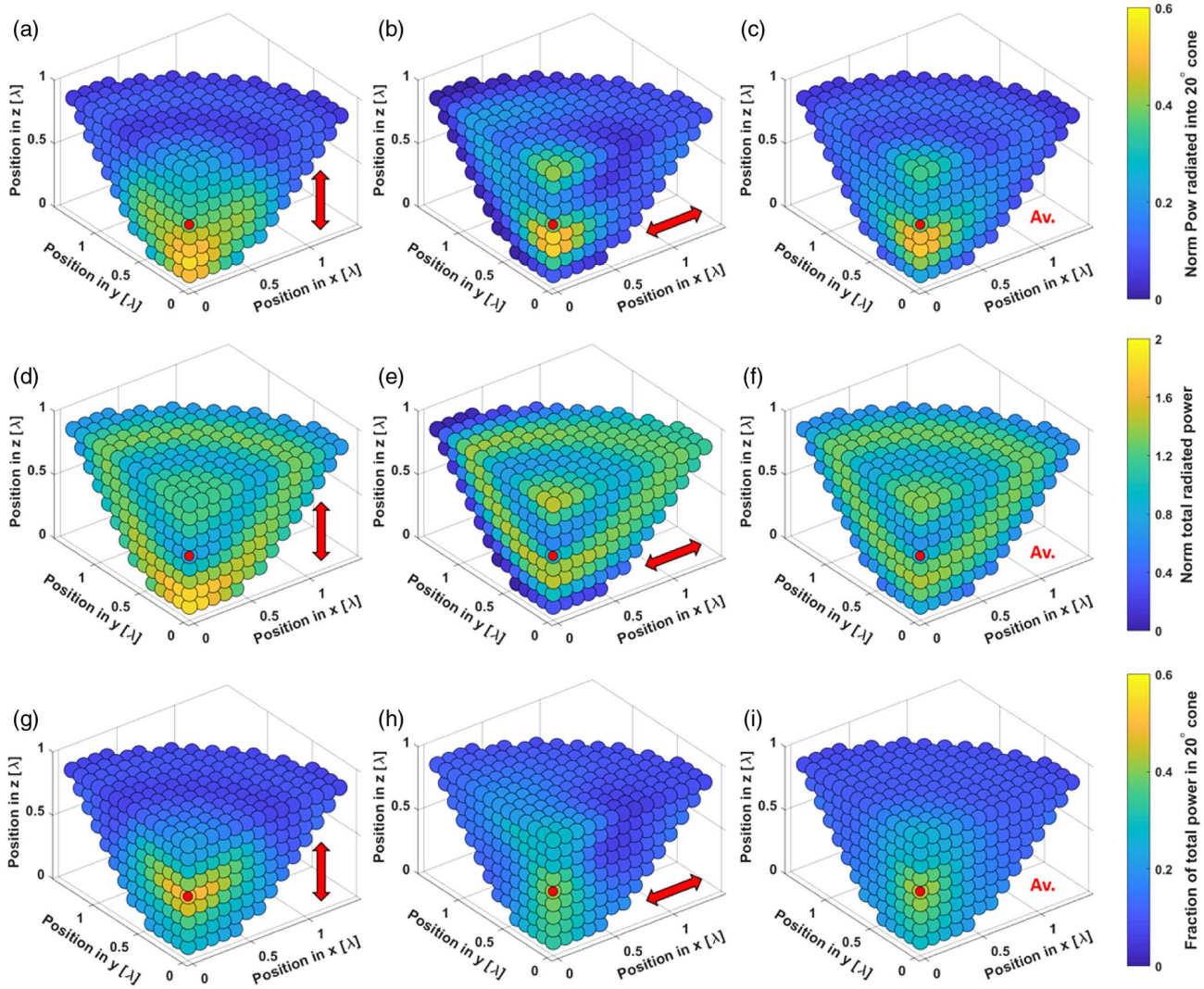

Fig. 4. Directed power for dipole emitters as a function of their position within a wavelength-scale parabolic reflector (top row), corresponding total radiated power (middle row), and fraction of total radiated power within the target cone (bottom row). The emission wavelength $\lambda = 600$ nm. The dipole orientation is given by the red arrows, where Av. denotes the geometric mean of the three orthogonal dipole orientations (where the dipole oscillation in the y case is obtained from the oscillation in the x solution shown). In (a)–(c) the power directed into a 20° half-angle cone is normalized to the total power emitted in the absence of any reflector, as is the total radiated power (d)–(f). Results for dipoles orientated in the $\hat{z}$ direction and the geometric mean possess rotational symmetry about the z axis, while perpendicular orientations have symmetry about the $x = 0$ and $y = 0$ planes. Red dots indicate the geometrical focal point of the paraboloids.

Results were therefore obtained for different electric dipole moment orientations.

Figures 4(a)–4(c) show the position-dependent power radiated into a 20° half-angle cone for dipole moments oscillating in the (a) vertical $\hat{z}$ and (b) horizontal $\hat{x}$ directions; (c) shows the geometric mean of the solutions for the three basis dipole moment orientations ($\frac{1}{3}\hat{x} + \frac{1}{3}\hat{y} + \frac{1}{3}\hat{z}$). It can be seen in (c) that the maximum power radiated into the target cone is approximately 50% of the total power radiated by an equivalent emitter in free space. As one would expect, this value falls short of the ∼75% achieved in the geometrical optics regime, which ignores diffraction. It can also be seen that while in the macroscale solution of Fig. 3 only a small improvement is gained by repositioning sources below the focal point, for the geometry chosen in Fig. 4 the geometrical focus is one of the worst possible choices.

In the COMSOL simulations we observe that for some emitter positions as much as 10% of the total power radiated was into directions below the reflecting surface. This power, which cannot have passed through the perfect electric conductor boundary condition corresponding to the metal, is attributed to the finite nature of the metallic surface surrounding the opening of the reflector [19]. As discussed, a finite metallic "surrounding" was a requirement of COMSOL's Stratton–Chu-based near-to-far-field transformation [15,16].

The maxima and minima present in Figs. 4(a)–4(c) can be understood by examining the spatial variation in the density of optical states, shown via the changes in total emitted power. Figures 4(d)–4(f) are equivalent to their top row counterparts, but they display the total power emitted for each source position and orientation. It can be seen that the poor performance around the focal position in Figs. 4(a)–4(c) can be attributed

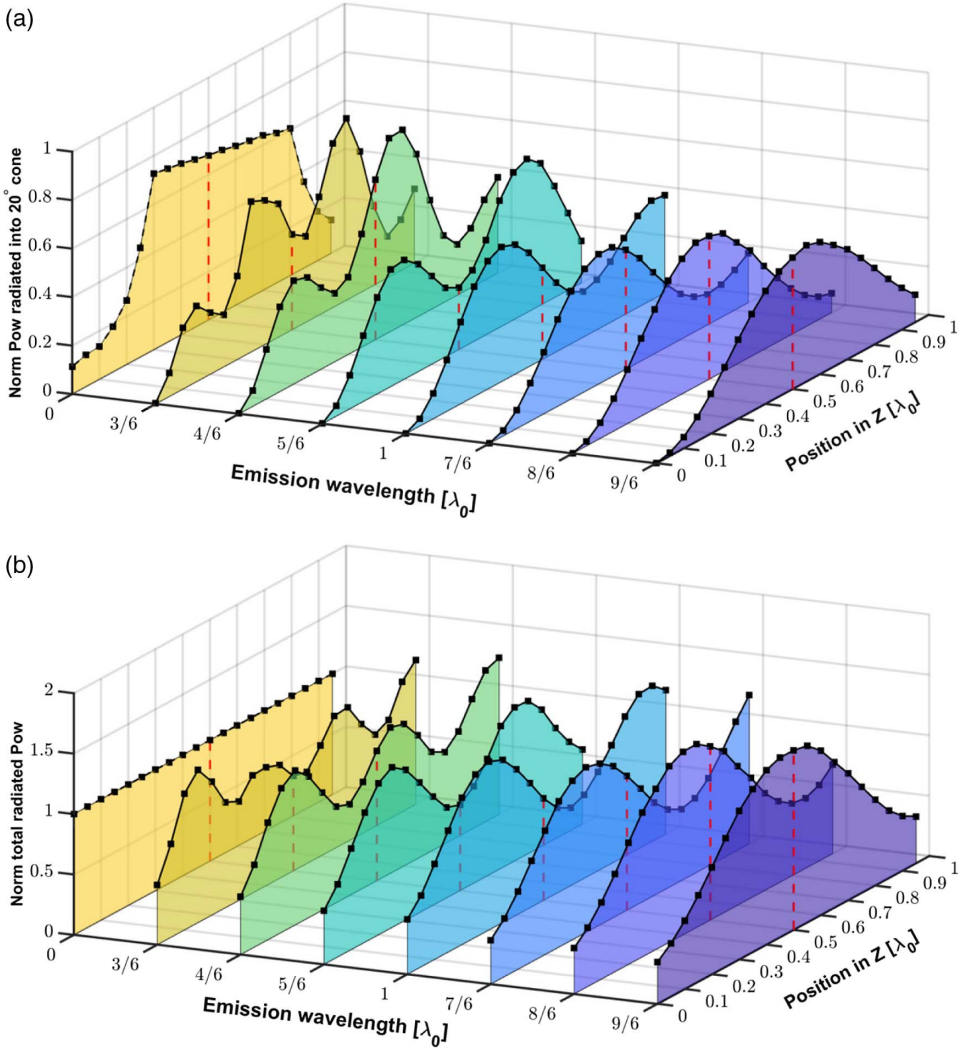

Fig. 5. (a) Variation in the power directed into a 20° half-angle cone with emitter position along the reflector's central axis and with emission wavelength. The emission wavelength is given in units of the design wavelength $\lambda_0 = 600$ nm, which determines the (fixed) size of the reflector. The size and shape of the reflector remains as in Fig. 4, with a vertex to opening distance of $\lambda_0 = 600$ nm. Directed power values are normalized to the total power radiated by an equivalent emitter (at the specified emission wavelength) in free space. The black squares indicate values obtained by simulation, and the connecting black lines are visual guides. The dashed red lines indicate the position of the geometrical focus. The "$\lambda = 0$" values represent the solution in the small wavelength limit in which the geometrical optics approximation may accurately be applied, and the solution does not depend on wavelength. (b) As in (a), but showing the total radiated power.

to a considerable reduction in the DOS here, compared both with its free-space value and more noticeably with the elevated DOS above and below the focal position. It can also be seen in Figs. 4(d) and 4(e) that the variations in the DOS follow intuitively from the case of an oscillating dipole above an infinite ground plane [20–23]. In this simplified case, consideration of the image charges induced in the mirror by the dipole provides an intuitive explanation. For a dipole oscillating immediately above and parallel to a mirror, the induced image charges effectively cancel out the dipole moment, whereas for a perpendicular dipole its effective moment is increased. This behavior is clearly seen for emitters close to the reflector in Figs. 4(d) and 4(e).

Figures 4(g)–4(i) show the fraction of total emitted power that is coupled into the target cone. This shows the results of the top row for directed power, normalized to the total radiated power of the middle row, as opposed to the power radiated in free space. This allows one to independently see the effects of the changes in the DOS and the "focusing ability" of the reflector, which combine to yield the directed power behavior seen in Figs. 4(a)–4(c). As one might expect, the focusing behavior seen in Fig. 4(i) is less pronounced and less spatially localized than that seen in the geometrical optics regime of Fig. 3.

Figure 4 shows that at this scale the local DOS has a strong bearing on both the optimum emitter position and the corresponding value for the directed power. As the size of the reflector is varied, so too will be the local DOS. Figure 5(a) shows the amount of power directed into a 20° half-angle cone for emitter positions along the central axis of the reflector, for a range of emission wavelengths, effectively varying the reflector size. The geometrical optics solution is present at the lambda = 0 position, for comparison. It can be seen that as the effective size of the antenna decreases, maxima in the directed power broaden and decrease in number. The expected trend of a general decrease in directed power with decreasing effective size is also observed, but has its exceptions as it competes with the changing location of maxima and minima in the DOS. Figure 5(b) shows the variation of the total emitted power (DOS).

The impact of the DOS on the directed power can clearly be seen by comparison of Figs. 5(b) and 5(a). For a $\lambda:\lambda_0$ ratio of 4/6, the directed power can be seen to exceed the optimal value obtained in the geometrical optics regime. This occurs for an emitter positioned 7/10 of the way from paraboloid vertex to the opening, over half an emission wavelength above the optimum inferred from geometrical optics.

4. CONCLUSIONS

It has been shown through numerical calculation that for parabolic antennas whose characteristic size is approximately the emission wavelength, the optimum emitter position deviates considerably from the paraboloid's focus. An informed choice on placing the emitter allows the power emitted into a cone to exceed the optimum value for the geometrical optics solution. In contrast, choosing to position the emitter at the focus may result in less than 50% of the directed power expected from geometrical optics. In summary, our results show that there is considerable scope to optimize the performance of wavelength-scale parabolic reflectors.

Funding. Engineering and Physical Sciences Research Council (EP/L015331/1).

Acknowledgment. We thank I. R. Hooper and T. A. Starkey for fruitful discussions. We acknowledge financial support from Dyson. We acknowledge support from the Engineering and Physical Sciences Research Council (EPSRC) of the United Kingdom, via the EPSRC Centre for Doctoral Training in Metamaterials. Data created during this research are openly available from the University of Exeter's institutional repository at https://doi.org/10.24378/exe.1883.

REFERENCES

1. C. Spencer, "Headlamp developments with DMC reflectors including homofocal arrangements," in *SAE Technical Paper* (1984), paper 840041.
2. C. A. Balanis, *Antenna Theory*, 3rd ed. (Wiley, 2005).
3. M. A. Lieb and A. J. Meixner, "A high numerical aperture parabolic mirror as imaging device for confocal microscopy," Opt. Express **8**, 458–474 (2001).
4. J. Stadler, C. Stanciu, C. Stupperich, and A. J. Meixner, "Tighter focusing with a parabolic mirror," Opt. Lett. **33**, 681–683 (2008).
5. S. Morozov, M. Gaio, S. A. Maier, and R. Sapienza, "Metal-dielectric parabolic antenna for directing single photons," Nano Lett. **18**, 3060–3065 (2018).
6. D. T. Schoen, T. Coenen, F. J. Garc, M. L. Brongersma, and A. Polman, "The planar parabolic optical antenna," Nano Lett. **13**, 188–193 (2013).
7. N. H. Wan, B. J. Shields, D. Kim, S. Mouradian, B. Lienhard, M. Walsh, H. Bakhru, T. Schröder, and D. Englund, "Efficient extraction of light from a nitrogen-vacancy center in a diamond parabolic reflector," Nano Lett. **18**, 2787–2793 (2018).
8. A. W. Schell, T. Neumer, Q. Shi, J. Kaschke, J. Fischer, M. Wegener, and O. Benson, "Laser-written parabolic micro-antennas for efficient photon collection," Appl. Phys. Lett. **105**, 231117 (2014).
9. J. P. Dowling, "Spontaneous emission in cavities: How much more classical can you get?" Found. Phys. **23**, 895–905 (1993).
10. E. Snoeks, A. Lagendijk, and A. Polman, "Measuring and modifying the spontaneous emission rate of erbium near an interface," Phys. Rev. Lett. **74**, 2459–2462 (1995).
11. M. Wubs and W. L. Vos, "Förster resonance energy transfer rate in any dielectric nanophotonic medium with weak dispersion," New J. Phys. **18**, 053037 (2016).
12. R. R. Chance, A. Prock, and R. Silbey, "Molecular fluorescence and energy transfer near interfaces," Adv. Chem. Phys. **37**, 1–65 (1978).
13. R. Sprik, B. A. van Tiggelen, and A. Lagendijk, "Optical emission in periodic dielectrics," Europhys. Lett. **35**, 265–270 (1996).
14. COMSOL AB, COMSOL Multiphysics.
15. J. Straton and I. Chu, "Diffraction theory of electromagnetic waves," Phys. Rev. **56**, 99–107 (1939).
16. COMSOL, The RF module user guide (2012).
17. D. K. Cheng, *Field and Wave Electromagentics*, 2nd ed. (Addison-Wesley, 1991).
18. R. K. Wangness, *Electromagnetic Fields*, 2nd ed. (Wiley, 1986).
19. Z. Živkovi, D. Senic, C. Bodendorf, J. Skrzypczynski, and A. Šaroli, "Radiation pattern and impedance of a quarter wavelength monopole antenna above a finite ground plane," in *20th International Conference on Software, Telecommunications and Computer Networks (SoftCOM)* (2012), pp. 1–5.
20. K. H. Drexhage, "Influence of a dielectric interface on fluorescence decay time," J. Lumin. **1-2**, 693–701 (1970).
21. S. Haroche, "Cavity quantum electrodynamics," in *Fundamental Systems in Quantum Optics* (North-Holland, 1992), Chap. 13, pp. 768–940.
22. W. L. Barnes, "Fluorescence near interfaces: the role of photonic mode density," J. Mod. Opt. **45**, 661–699 (1998).
23. H.-S. Ee, S.-K. Kim, S.-H. Kwon, and H.-G. Park, "Design of polarization-selective light emitters using one-dimensional metal grating mirror," Opt. Express **19**, 1609–1616 (2011).